LAWRENCE
LIVERMORE
NATIONAL
LABORATORY

UCRL-JRNL-233057

The Effect of Polarizability for the Understanding the Molecular Structure of Aqueous Interfaces

C. D. Wick, I. W. Kuo, C. J. Mundy, L. X. Dang

July 25, 2007

Journal of Chemical Theory and Computation

Disclaimer

The Effect of Polarizability for the Understanding the Molecular Structure of Aqueous Interfaces

Collin D. Wick,[1] I-Feng W. Kuo,[2] Chris Mundy,[1] and Liem X. Dang[1]

[1]Pacific Northwest National Laboratory,

Richland, WA, 99352.

[2]Lawrence Livermore National Laboratory,

Livermore, CA 94550

Abstract

A review is presented on recent progress of the application of molecular dynamics simulation methods with the inclusion of polarizability for the understanding of aqueous interfaces. Comparisons among a variety of models, including those based on density functional theory of the neat air-water interface are given. These results are used to describe the effect of polarizability on modeling the microscopic structure of the neat air-water interface, including comparisons with recent spectroscopic studies. Also, the understanding of the contribution of polarization to the electrostatic potential across the air-water interface is elucidated. Finally, the importance of polarizability for understanding anion transfer across an organic-water interface is shown.

Introduction

Aqueous interfaces are ubiquitous in nature, and pose characteristics that affect countless biological, atmospheric, pharmaceutical, and industrial processes. These processes are dependent on the molecular level details of these interfaces, and are manifested in enhanced or depleted molecular activity and reaction rates at interfaces, detergent agent, membrane permeability, and molecular uptake in aqueous aerosols. Because of this, there is a strong effort to understand the molecular level properties of these interfaces. This understanding is beginning to form due to, in part to the introduction of polarizability in the molecular models used to study aqueous interfaces. Polarizability has been found to be of highest importance for the realization that some anions have a propensity for the interface.[1,2] However, the importance of polarizable interactions for understanding the properties of neat air-water interfaces is not comprehensive. In fact, while there is some indication of the importance for polarizability for the determination of thermodynamic properties at the air-water interface,[3] there is also some indication that polarizability is of secondary importance for air-water interfacial properties.[4,5]

In the past few years, there has been a large amount of surface sensitive spectroscopic techniques dedicated to studying the air-water interface.[6-12] The vibrational sum frequency generation spectroscopic (SFG) technique and the emerging area of X-ray techniques applied to liquid-vapor interfaces are elucidating significant details of the molecular structure of the air-water interface.[6,8-11,13] Experimental findings include both the characterization of a single donor (a free O-H vibration) and acceptor only (two free O-H stretches) hydrogen bond

species at the air-water interface, and thus fewer on average hydrogen bonds for interfacial waters than bulk ones.[14] Because of the heterogeneous nature of the interfacial region, it can be easily justified that the hydrogen bond populations and degree of hydrogen bonding will differ from their bulk values. However, the dependence of these populations on the interaction potential, and the ability to understand and agree with spectroscopic determinations of interfacial hydrogen bonding still a topic of debate.[9]

Recent X-ray absorption fine structure (EXAFS) experiments found another interesting feature, namely that there is an expansion in the average water oxygen-oxygen distances at the air-water interface when compared with the bulk.[7] A following computational study of the air-water interface found no expansion using a variety of classical force fields, but did find that with Car-Parinello molecular dynamics (CPMD), using density functional theory (DFT) with a BLYP exchange and correlation functional, surface expansion at the air-water interface was observed.[15,16] One may question as to what features are necessary in a classical molecular model to capture this experimentally observed surface relaxation.

The inclusion of polarizability may be the key for the observation of surface relaxation at the air-water interface. Two of the most common ways to account for polarizability for rigid water models are the fluctuating charge (FQ)[17] technique, and including explicit point polarizabilities. The important distinction between explicitly polarizable and FQ models is that for a polarizable model, a dipole is induced at one or more point polarizabilities based on the local electric field. For FQ water models, the local electric field induces a change in the charge distribution between the hydrogens and the oxygen or other non-atomic

interaction sites keeping an overall neutral molecule. Both techniques are designed to mimic charge reorganization in a water molecule in response to its solvation environment.

Another way to characterize interfaces is to determine the electrostatic potential across them.[18] The electrostatic potential can be used to characterize the distribution of electrostatic charge and thus the molecular structure at an interface. Although the empirical potentials cannot capture the true potential due to the nuclear charge and electrons, the value of the surface potential appears to be insensitive to the type of empirical interaction potential (*viz.* fix charge or polarizable).[19] With the inclusion of polarizability, the effect of specific molecular structures and orientations can be separated from effects due to rearrangement of charge in a molecule. However, the effects of a smeared charge distribution cannot be easily dismissed. It has been shown that for simple Gaussian model of charge smearing, the degree of smearing as determined by the width of the Gaussian, can have dramatic effects on the value of the surface potential.[20] Understanding the effect of polarization and a realistic charge distribution can be a major factor in interpreting electrostatic potential measurements.

While polarizability has been found to be paramount for understanding anions at air-water interfaces, only recently has polarizability been used to understand ions at organic-water interfaces.[21] With an organic (in this case CCl_4) present at the interface with water, the interfacial properties are different than at an air-water interface.[22] With these different interfacial properties, understanding if the effect of polarizability for organic-water interfaces is similar to that for ion transfer across air-water interfaces is of importance.

The paper is organized as follows. The next section gives details for some simulations carried out for this work. The results and discussion section gives a comparison of a variety of molecular models for understanding the air-water interface, followed by a discussion as to the relevance of polarizability to understanding interfacial electrostatic potentials. Then, the free energy profile of a polarizable hydronium molecule across an air-water interface is shown. Next, a comparison of the free energy profile for iodide across organic-water interfaces with and without polarizable interactions is given. Finally, a summary and conclusions are given.

Models and Simulation Details

Classical Simulations of Pure Water. Classical molecular dynamics (MD) simulations were carried out utilizing the rigid 4-site TIP4P,[23] rigid 4-site Dang-Chang[24] (D-C), and flexible 3-site SPC-FW[25] water models. The TIP4P and D-C water models are rigid with four interaction sites. All models contain a single Lennard-Jones interaction site located on the oxygen atomic position, and the SPC-FW model has a negative charge located at the oxygen position. All models have two hydrogen atomic sites with positive charges, and the TIP4P and D-C models have an additional *m* site located along their oxygen-hydrogen bisectors. For the TIP4P and D-C models, the *m* site contains a negative charge, but the D-C model has an additional point polarizability located on it. The point polarizability allows the formation of induced dipoles in response to the local electric field. Induced dipoles were evaluated by a self-consistent iterative procedure, which is described in detail elsewhere.[24] A potential truncation of 9 Å was employed for short-ranged interactions, and the particle mesh Ewald

summation technique was used to handle long ranged electrostatics.[26] For the SPC-FW model, since it is flexible, the RESPA algorithm was used with multiple timesteps,[27] with a timestep of 1 fs for intermolecular interactions, and a 0.01 fs timestep for bonded interactions.

A total of 1000 water molecules were set up in boxes in slab geometry with periodic liquid containing water molecules in the x and y directions, and elongated in the z direction, giving dimensions of 30 Å (x) × 30 Å (y) × 100 Å (z) . The amount of air volume was approximately double of the liquid volume for these simulations. Data was collected in a 500 ps production run for the D-C and SPC-FQ water models, and a 1 ns production run was carried out for TIP4P, both after extensive equilibration. The temperature was kept constant at 298 K with the Berendsen thermostat for TIP4P and D-C models,[28] and the SHAKE algorithm was used to keep the molecules rigid.[29] The SPC-FW model had its temperature kept constant with Nose-Hoover chains thermostat with one chain for each atom.[30]

Car-Parinello Molecular Dynamics of Neat Aqueous Liquid-Vapor Interface. The details for the Car-Parinello Molecular Dynamics (CPMD) simulations are described in detail elsewhere,[15,16,31] and only a brief overview is given here. The CPMD simulations perform density functional theory (DFT) based calculations with the BLYP exchange and correlation functional.[32,33] The system was set up in slab geometry with dimensions 15 Å (x) × 15 Å (y) × 71.44 Å (z), and 216 water molecules. A total of 10 ps of equilibration were carried out, and the results were obtained over 4 ps.

Results and Discussion

Density Profiles. The density as a function of z coordinate is given in FIG. 1 for the D-C, TIP4P, and BLYP simulation results. The density profiles were fit to a hyperbolic tangent to determine the Gibbs dividing surface (GDS) and to elucidate the interfacial width (δ).

$$\rho(z) = \frac{1}{2}(\rho_l + \rho_v) - \frac{1}{2}(\rho_l - \rho_v)\tanh\left(\frac{z - z_{\mathrm{GDS}}}{\delta}\right) \qquad (1)$$

where ρ_l and ρ_v are the average liquid and gas densities, respectively. Table 1 gives the average liquid densities and interfacial widths of the tested water models along with previously determined results[15] for the TIP4P-POL2[34] and TIP4P-FQ[17] water models. The TIP4P-POL2 and TIP4P-FQ models are 4-site water model, similar to D-C and TIP4P, but are FQ models instead of using point polarizabilities. While the densities of the TIP4P and D-C water models are indistinguishable, the interfacial length of the D-C water model is smaller than TIP4P. The interfacial length for the SPC-FW model is similar to that of D-C, and the interfacial widths for the FQ models are the greatest. The BLYP simulations are dominated by noise, resulting in an ice-like profile. However, this is only an artifact of the spatial and temporal sampling in the common procedure for computing density profiles. In a previous study, we have computed the Voronoi polyhedra for liquid water averaged over time.[15,16] This procedure only relies on the continuous particle positions and was shown to give identical fluctuations to those obtained with classical simulations. In the same study the short-time rotational dynamics of the water molecules at the surface and in bulk obtained with classical empirical and DFT interaction potentials were compared.[15] It was

found that the time-scale of the librational dynamics was nearly identical between models indicating the presence of a fluid state. However, it is still clear from examining the radial distribution functions obtained with BLYP in the interior regions of the interface yields an over structured water consistent with recent DFT calculations on bulk liquid water [35-39] There is still considerable speculation as to the exact cause of the observed over structuring obtained with DFT interaction potentials (*e.g.* system size, basis set, functionals, quantum effects). A recent study has shown that utilizing BLYP in the complete basis set limit can reduce the amount of overstructuring.[35] Another DFT study has shown that the use of hybrid density functionals containing exact exchange can also reduce the overstructuring.[36] One should be reminded that all of the aforementioned studies on the over structuring of liquid water as determined by the radial distribution function were performed at constant volume. The BLYP interface was not constrained to be at 1 g/cc leading to the calculated density to be less than 1 g/cc (see Figure 1). To investigate whether this is a result of poor sampling or simulation protocol, extensive Monte Carlo (both Gibbs' ensemble and NpT) were conducted to map out the liquid-vapor coexistence of liquid water utilizing at DFT interaction potentials.[40-43] These studies have all concluded that the density of liquid water at 298K and 1 atm is less that 1 g/cc in good agreement with the results obtained in the interior of the liquid-vapor interface. Furthermore, Monte Carlo studies using different functionals and basis-sets have been completed yielding the same qualitative conclusions that DFT interaction potentials yield a density of water that is less than 1 g/cc.[40] From these results, it is not clear how polarizability specifically affects the air-water interfacial width, δ. One should be reminded that the evaluation of δ using the

BLYP trajectory obtained by giving all points on in the density profile the same weight.[15] Thus, statistics will play a significant role in this number and it is more instructive to look at a variety of structural and electronic properties in order to synthesize a coherent picture of the effects of polarization on interfacial properties.

Dipole Distributions. The dipole distributions for the D-C, SPC-FW, and BLYP simulations are given in FIG. 2., with the average bulk dipole, along with the average dipole at the GDS for a variety of water models given in Table 1. For all polarizable models and BLYP, the dipole decreases somewhat from the bulk to the GDS, and drops off to much lower values outside the GDS. The experimental value of 2.9 ± 0.6 for bulk water[44] is in agreement with all of the models shown, except TIP4P, which is outside of this range. The BLYP has the greatest decrease in dipole from the bulk to the GDS. Because DFT interaction potentials do not contain dispersion outside of the interaction energy due to overlapping charge densities, all of the interaction is governed by electrostatics. Thus, the large drop in dipole moment in the vicinity of the interface will give rise to a dramatic loss in the interaction energy, which may account for the surface expansion seen in DFT models of the aqueous liquid-vapor interface. For the classical force fields, the TIP4P-POL model has the smallest drop, while the TIP4P-FQ model has the largest drop (D-C is in between them). Apparently, the type technique used to model charge rearrangement does not significantly affect the change in water dipole as it approaches the interface. It should be noted that while flexible water models have significantly different dipoles in the gas and liquid phases,[25] there is

very little difference between the bulk and the interface in the molecular dipole for SPC-FW, which is at odds with the DFT interaction potentials.

Water Electrostatic Potential. The electrostatic potential (EP) from atomic charges ($\Delta\phi_q(z)$) can be determined from the integral of the electric field from some reference point in the vapor (z_0) across the air-water interface into the water bulk,[20,45]

$$\Delta\phi_q(z) = \phi_q(z) - \phi_q(z_0) = \int_{z_0}^{z} \mathrm{E}_q(z')\mathrm{d}z' \tag{2}$$

The electric field due to fixed charges (E_q) is determined from the integral of charge density as a function of position ($\rho_q(z')$),

$$\mathrm{E}_z(z) = \frac{1}{\varepsilon_0}\int_{z_0}^{z} \left\langle \rho_q(z') \right\rangle \mathrm{d}z' \tag{3}$$

where ε_0 is the permittivity of vacuum, and the brackets denote an ensemble average for a liquid slab of 0.5 Å width. Equation 2 gives the total electrostatic potential for the TIP4P water model. For polarizable models, such as D-C, an additional contribution comes from the induced dipoles,[19]

$$\Delta\phi_\mu^{\mathrm{ind}}(z) = \phi_\mu^{\mathrm{ind}}(z) - \phi_\mu^{\mathrm{ind}}(z_0) = \frac{1}{\varepsilon_0}\int_{z_0}^{z} \left\langle \rho_\mu^{\mathrm{ind}}(z') \right\rangle \mathrm{d}z' \tag{4}$$

where ρ_μ^{ind} is the induced dipole density. The EPs from static charges and induced dipoles for the TIP4P and D-C molecular models are given in FIG. 3. The total EPs for both classical models are quite similar, around -0.5 V, with TIP4P being slightly greater in magnitude. Experimental values suggest that the surface potential for neat water is likely positive,[46] in disagreement with the

results here. Wilson *et. al*. found that smearing the charges in a Gaussian distribution results in an increase in surface potential to positive values,[20] which if applied to the results here, could result in positive surface potential values. The EP for DFT BLYP simulations are underway and will directly address the effects of charge transfer and smeared charge distribution on the calculated surface potential.

The agreement with TIP4P and D-C, along with a large number of classical potentials giving similar EP values[45] suggests that polarizability has little effect on the total EP if the bulk phase properties are similar. For the D-C model, though, the EP is distributed among static charges and induced dipoles. The orientation of the TIP4P and D-C models with respect to the surface normal are related to their static EPs. When the static EP decreases from left to right, the water hydrogens are pointing towards the water bulk, and when the EP increases, they are pointing primarily towards the vapor. In the region between 0 and 5 Å from the GDS, the two models' static EP are nearly identical, showing a similar orientation. Where the models differ significantly in static EP, though is in the region between 0 and -5 Å from the GDS. In this region, both models show a general decrease in static EP, but the D-C model shows this to a much greater degree. This corresponds to D-C waters orienting their hydrogens in this region towards the water bulk to a much greater degree than TIP4P. It should be noted that this orientation of the water dipoles is consistent with second harmonic generation results.[12]

Interfacial Water Orientation. To better elucidate the orientation of interfacial water molecules, the distribution of the angle the water oxygen-hydrogen vector forms with respect to the surface normal is given in FIG. 4 for both hydrogen-bonded and non-hydrogen-bonded (free) hydrogens. The criteria for a hydrogen bond are described in the next section. The first point of interest is the fact that the free hydrogen orientations are very similar between the D-C and TIP4P models, showing very strong orientation of the free hydrogen towards the vapor, in agreement with many experimental observations. [8-11] There is a noticeable difference between the two models in that the point where the free hydrogen points towards the interface for TIP4P is shifted slightly more towards interior than D-C. The most pronounced difference between the two models, though, is present with the hydrogens that are involved in H-bonds. In the region between -2.5 Å and greater, the D-C model clearly shows a greater orientation of its H-bonded hydrogens towards the liquid interior. This is similar to the observation shown in the electrostatic potentials of the two models. The strong decrease in the D-C EP with respect to TIP4P in FIG. 3 between -5 and 0 Å is shown to be the result of a combination of a decrease in the propensity for a non-H-bonded hydrogen to point towards the vapor along with an increase in the propensity for an H-bonded hydrogen to point towards the interior.

Hydrogen Bond Populations. The hydrogen bond populations in the water bulk and at the interface are given in Table 2. The criteria for hydrogen bonding are a combination of an intermolecular oxygen-hydrogen distance less than 2.27 Å and an oxygen-hydrogen-oxygen angle greater than 150°. Previous studies found

that the qualitative trends between the interface and the bulk are similar between this criteria and many others.[15] The interfacial region defined here is considered to be 2*d* from the GDS for TIP4P and D-C. Since the *d* value for the BLYP simulations was much smaller than the other two systems, a value of 1.61 Å (same as a previous paper with BLYP)[15] was used for this study to be similar to the other two. To make better comparisons between the different simulation results, FIG. 5 gives the ratio of bulk to interfacial hydrogen bond populations for D-C, TIP4P, and BLYP. It should be noted that the symbol for 1 donor and 2 acceptors for the D-C model (black square in right column) is overlapped by the result for TIP4P (red square). The first noticeable trend is that for most cases, the ratio for D-C is shifted towards the BLYP results from the TIP4P (i.e. the D-C ratio is closer to the BLYP ratio for most cases). The ratios for all entrees are largest for the TIP4P water model except the case with 2 donors and 2 acceptors, in which TIP4P is the smallest. From these results, it can be inferred that the inclusion of polarizability decreases the number of fully coordinated hydrogen bonding waters at the interface. However, the overall population trends in the water bulk are independent of the type of interaction potential.

Surface Relaxation. One interesting feature that has been recently observed experimentally using the EXAFS technique is that the oxygen-oxygen distance expands at the interface with respect to the bulk.[7] The concept of surface relaxation is not new and is studied extensively in the solid state physics community where surface relaxation effects are known do be due to charge rearrangement of unsatisfied bonds at solid-vapor interface. Quantifying surface

relaxation in a disordered system is much more difficult. The only reporting of this quantity using computational models, to our knowledge, showed that surface relaxation at the neat liquid-vapor interface has not been observed with any classical force fields, including FQ models. However, as previously mentioned, surface relaxation was observed using DFT interaction potentials in conjunction with BLYP exchange and correlation functional.[15,16] Here we present the running average oxygen-oxygen distance (r_{OO}) as a function of position for the models tested in this review (FIG 6). Table 3 gives the average value at the bulk and interface for models considered in the review to be compared to the data in Ref 15. All water models show a contraction at the interface, with exception of the D-C model and the BLYP results. It is interesting that the D-C model provides an outward expansion that is qualitatively similar to BLYP and experiment, unlike all the other models tested. The values shown in Table 3 for BLYP and D-C show only a very small increase in r_{OO} corresponding to 1% and 0.3%, respectively, at the GDS. This is much lower than the experimental expansion of 5.9%.[7] However, FIG. 6 shows that outside the GDS, further expansion of the r_{OO} distances occur, leading to increases of 2.4% and 2.9% at 5 Å for BLYP and D-C, respectively, closer to experiment. In order to make quantitative contact with experiment, the calculation of the surface versus bulk EXAFS spectra needs to be computed. This is work that is currently underway using representative configurations from the D-C and DFT-BLYP interface calculation in conjunction with the FEFF code to compute the EXAFS spectra. It should be noted that two of the models, the TIP4P-FQ and SPC-FW, do have versions that include polarizability.[47,48]

Electrostatic Potentials For Salt and Acid Solutions. The simulated EPs for 1M KCl[49] and 1M HCl solutions with polarizable models were determined. The 1M HCl solution used 48 classical polarizable hydronium ions,[50] 48 polarizable chloride ions,[51] and 1000 D-C water molecules. These EP results were obtained from 1 ns of simulation time. The total EPs for pure water, 1M KCl, and 1M HCl solutions is given in FIG. 7. The addition of KCl salt increases the surface potential, in agreement with experimental observations.[18]

The decomposition of the EP into contributions from static charges and induced dipoles is given in FIG. 8. The static EP drops originally due to dangling hydrogens from the water molecules, as is the case for pure water, followed by a significant increase in static EP. This increase in static EP is due to the anisotropic pairing of KCl at the interface. The computed density profiles for the 1M KCl salt solutions confirmed this, by showing the higher anion concentration near the GDS (not shown).[49] Also, it showed an increase in K^+ density between –5 and –7.5 Å from the GDS, just next to the region where Cl^- density is greater than K^+ density. This double layer creates a dipole at the surface pointing towards the gas phase, which contributes negatively to the electric field and positively to the static EP from the vapor to the liquid. The induced dipole EP works against the static EP, being significantly negative in value. The result is that the total EP is negative, but more positive than for pure water. It should be noted that if the total EP was used as a gauge to understand ion pairing at the interface, it would significantly underestimate the true amount of ion pairing, since it doesn't take into account the effect of induced polarization.

The computed surface potential for 1M HCl is also included in FIG. 7. Upon examining the results, there are several observations that are in order: 1) the shift in the surface potential of 1M HCl is larger than the corresponding 1M KCl, which is consistent with experiment,[18] 2) this larger shift is probably due to in part to the presence of the hydronium ions at the interface. This observation is demonstrated in the snapshots taken from MD simulations shown in FIG. 9.

To bring insight into hydronium interfacial activity, its free energy profile using the constrained molecular dynamics potential of mean force (PMF) technique. The PMF technique drags a molecule across an interface, constraining the molecule position and liquid center of mass. The force acting between the constrained liquid and molecule is recorded as a function of *z* position, yielding a free energy profile across the interface,

$$\Delta F(z_s) = F(z_s) - F_0 = \int_{z_0}^{z_s} \langle f_z(\zeta) \rangle \mathrm{d}\zeta \qquad (5)$$

For this work, a single hydronium ion was dragged in 1 Å increments across an air-water interface with 1000 water molecules. FIG. 10 gives the free energy profile as a function of position for the hydronium across the air-water interface. As conjectured above, the PMF shows a free energy minimum at the interface, showing a propensity for the hydronium for the air-water interface, in agreement with recent nonpolarizable simulation results[52] and experimental[53] results.

Ion Transfer Across Organic-Water Interfaces. A recent study of the transfer of iodide across the organic-water interface compared the free energy profile with polarizable and non-polarizable models.[54] The simulations with polarizable models used the D-C water model,[24] a polarizable CCl_4 model,[22] and a polarizable

iodide.[51] The simulations with non-polarizable models included the TIP4P water model,[23] OPLS CCl_4 model,[55] and a non-polarizable iodide.[19] The free energies for the polarizable and non-polarizable models using the PMF technique are shown in FIG. 11. There is a clear free energy minimum for the simulations with polarizable model between -2.5 and 0 Å of the GDS, which is not present with the non-polarizable model. This minimum in the free energy at the water interface that was only present when using polarizability is slightly shallower than that calculated for the air-water interface.[19] What is clear, though, is that the inclusion of polarizability is paramount for the understanding of ion transport across organic-water interfaces, just as it was found for the air-water interface.

Conclusions

We presented a review on recent progress of the application of molecular dynamics simulation methods, including which polarizable potential models were used, to describe interactions among species, and how they affect a variety of chemical and physical processes at interfaces. It was found that polarizability played an important role for determining the molecular structure and orientation at neat air-water interfaces, including observing surface relaxation at the air-water interface. To our knowledge, only BLYP and Dang-Chang have been shown to result in an expansion at the air-water interface, but it should be stated that other models, especially those with polarizability, would likely show this also. In addition, the effect of polarizability on the understanding of electrostatic potential across the air-water interface, and how it is influenced by the addition of KCl salt and HCl acid is important. Finally, only with the inclusion of

polarizability, the free energy profile of iodide was shown to have a minimum at the organic-water interface.

Acknowledgements

This work was performed at Pacific Northwest National Laboratory (PNNL) under the auspices of the Division of Chemical Sciences, Office of Basic Energy Sciences, U.S. Department of Energy. PNNL is operated by Battelle.

This work performed under the auspices of the U.S. Department of Energy by Lawrence Livermore National Laboratory under Contract DE-AC52-07NA27344.

Figure Captions

FIG. 1. Density profiles for the simulation results for BLYP, TIP4P, D-C, and SPC-FW. Zero in the *z*-axis represents the GDS for all figures.

FIG. 2. Average dipole as a function of *z* position for models described in FIG. 1.

FIG. 3. Electrostatic potentials across the air-water interface for the TIP4P and Dang-Chang (D-C in figure) water models, including contributions from static charges and induced dipoles for Dang-Chang.

FIG. 4. Average oxygen-hydrogen angle with the surface normal, with positive values corresponding to hydrogens pointing away from the water center of mass for the models in FIG. 1.

FIG. 5. Ratio of bulk to interfacial hydrogen bond populations for the D-C (black), TIP4P (red), and BLYP (green) results as a function of the number of hydrogen bond donors and acceptors.

FIG. 6. Average first solvation shell oxygen-oxygen distance for water as a function of position.

FIG. 7. Electrostatic potentials using polarizable models for water, 1M KCl and 1M HCl.

FIG. 8. Decomposition of electrostatic potential into contributions from static charge and induced dipoles.

FIG. 9. Snapshots taken from MD simulations of 1M KCl and 1M HCl.

FIG. 10. Free energy for transferring a hydronium ion across the air-water interface with polarizable potential models.

FIG. 11. Free energy profile of the transfer of iodide across the H_2O-CCl_4 interface for polarizable (pol) and non-polarizable (non-pol) models.

Figures

FIG. 1.

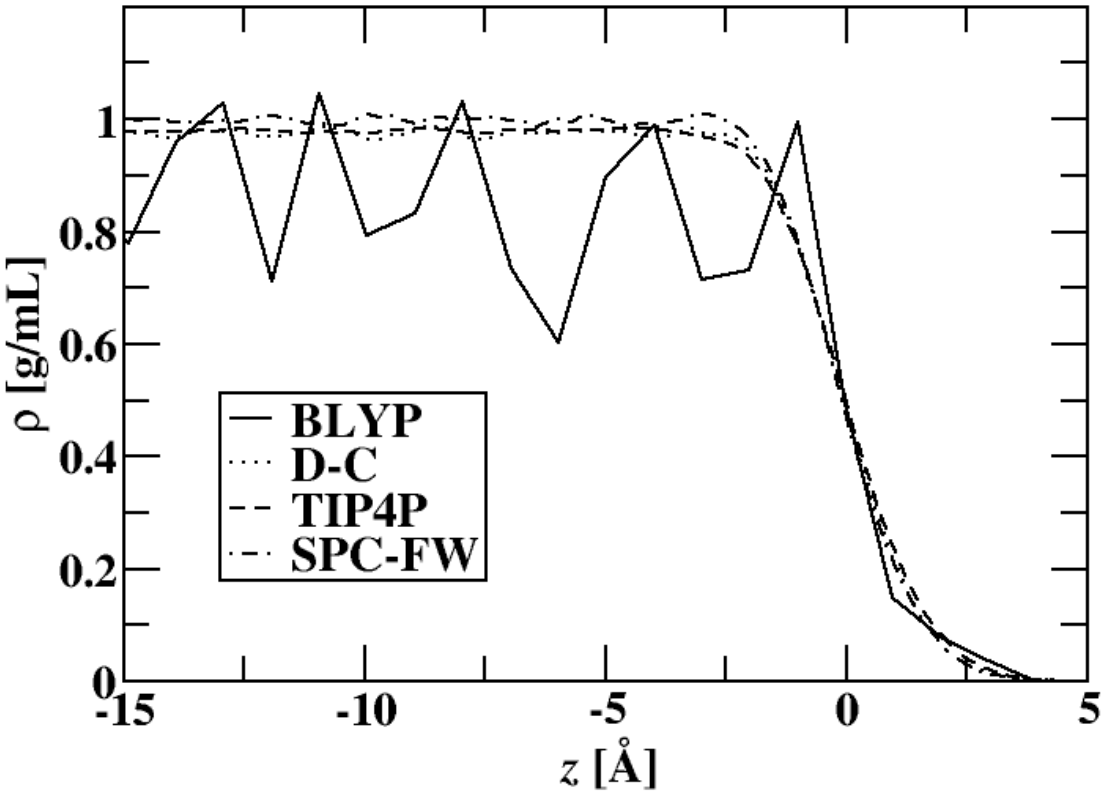

FIG. 2.

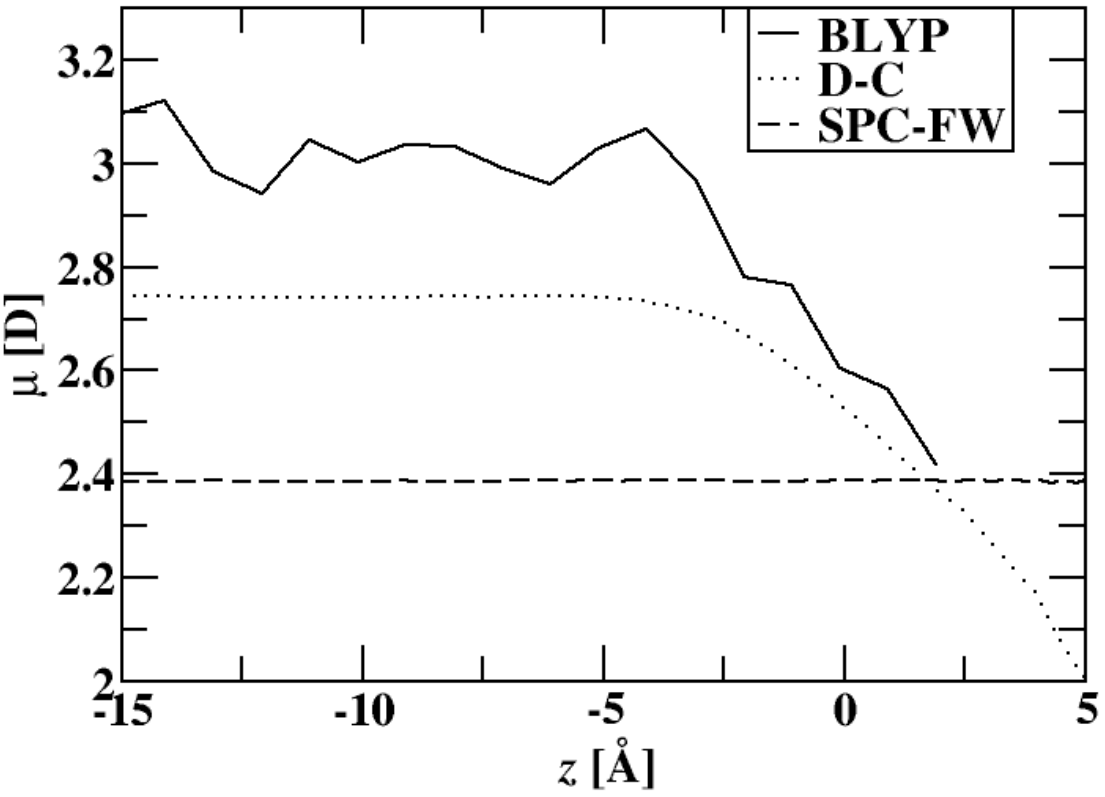

FIG. 3.

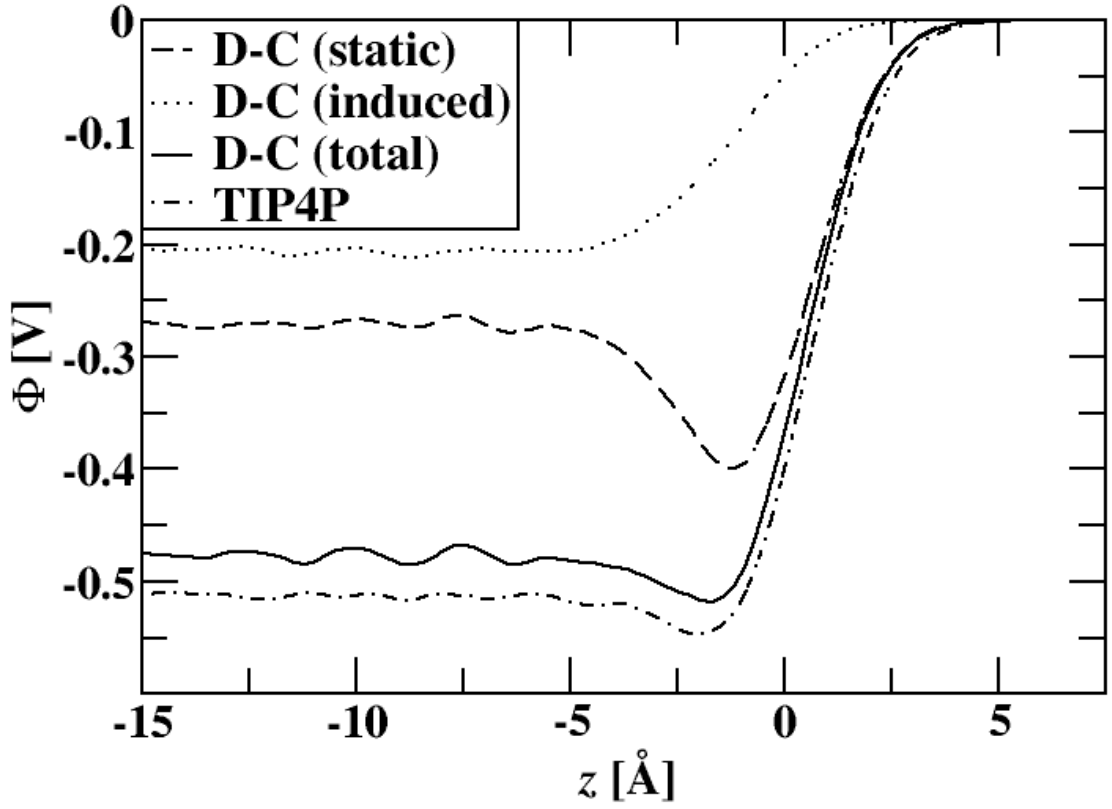
D-C (static)
D-C (induced)
D-C (total)
TIP4P
0
-0.1
-0.2
-0.3
-0.4
-0.5
Φ [V]
-15
-10
-5
0
5
z [Å]

FIG. 4.

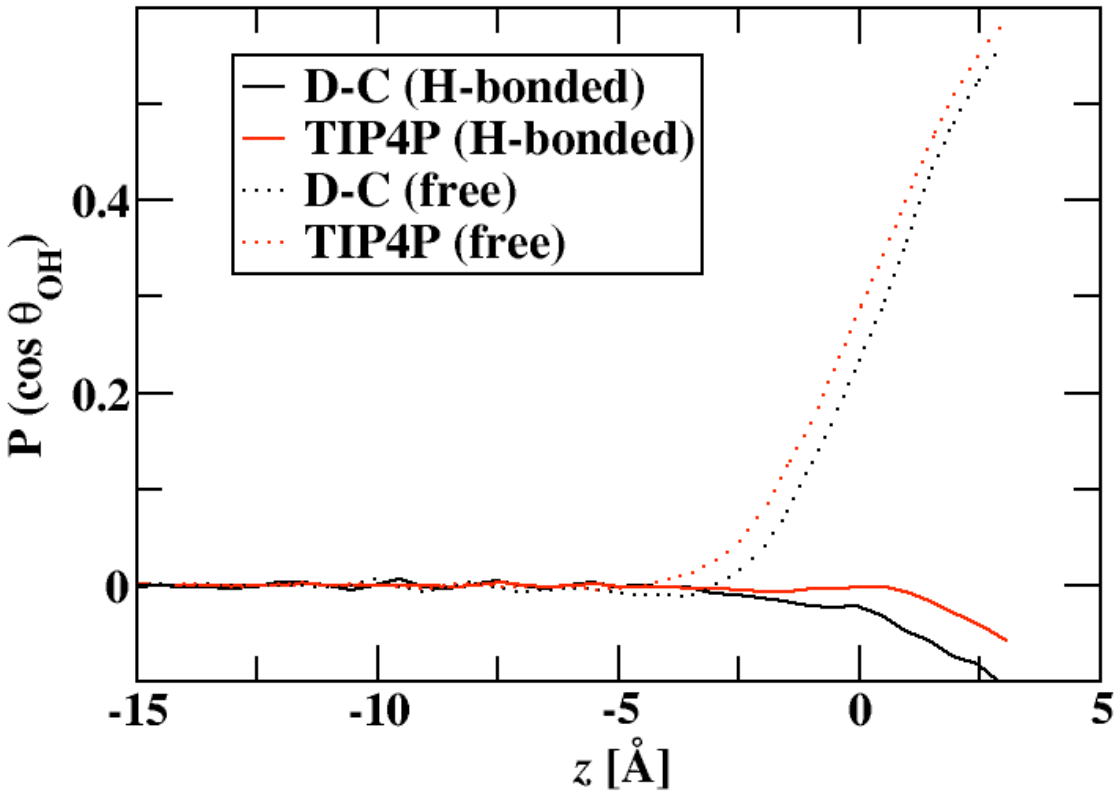
D-C (H-bonded)
TIP4P (H-bonded)
D-C (free)
TIP4P (free)
P (cos θ_OH)
0.4
0.2
0
-15
-10
-5
0
5
z [Å]

FIG. 5.

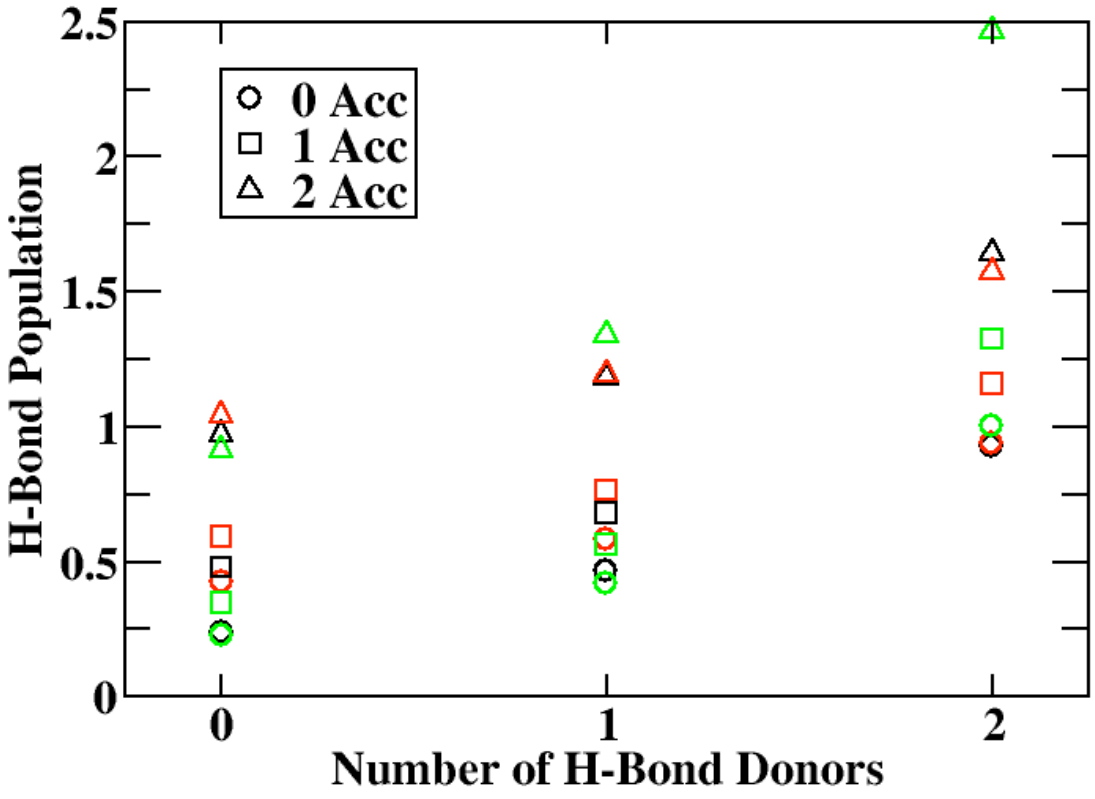
2.5
2
1.5
1
0.5
0
H-Bond Population
0 Acc
1 Acc
2 Acc
0
1
2
Number of H-Bond Donors

FIG. 6.

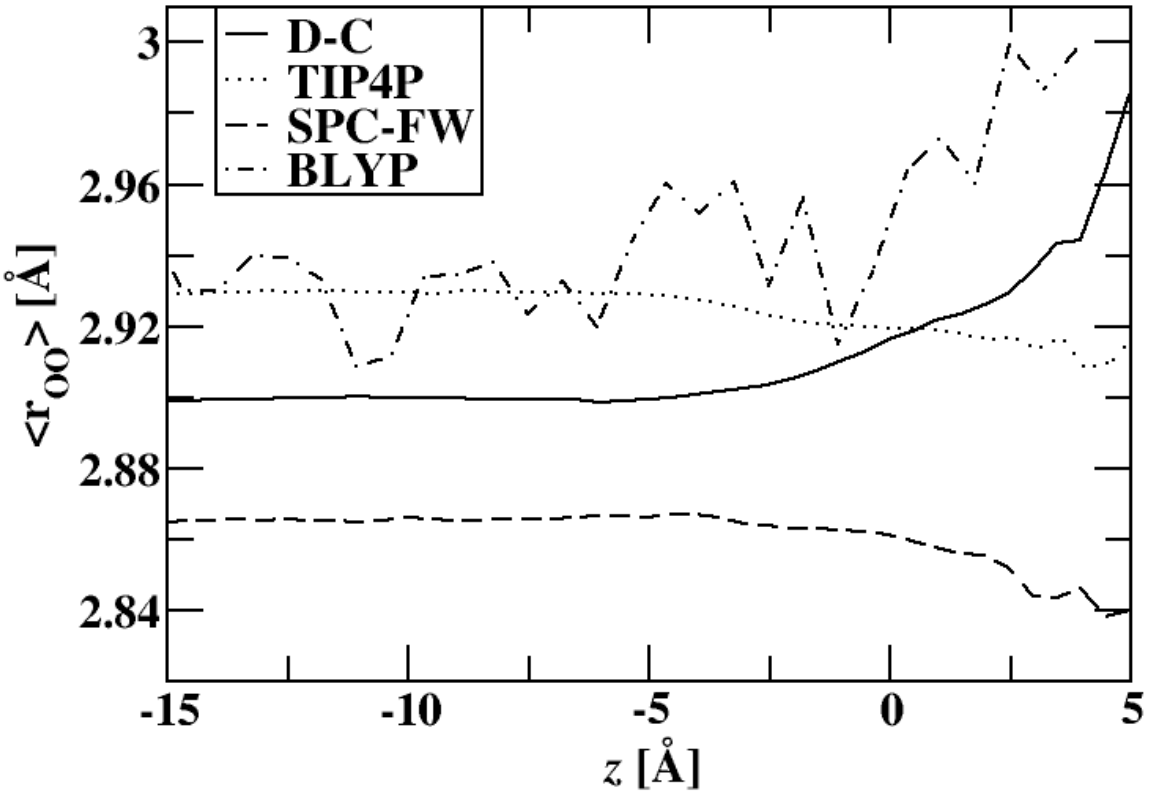

FIG. 7.

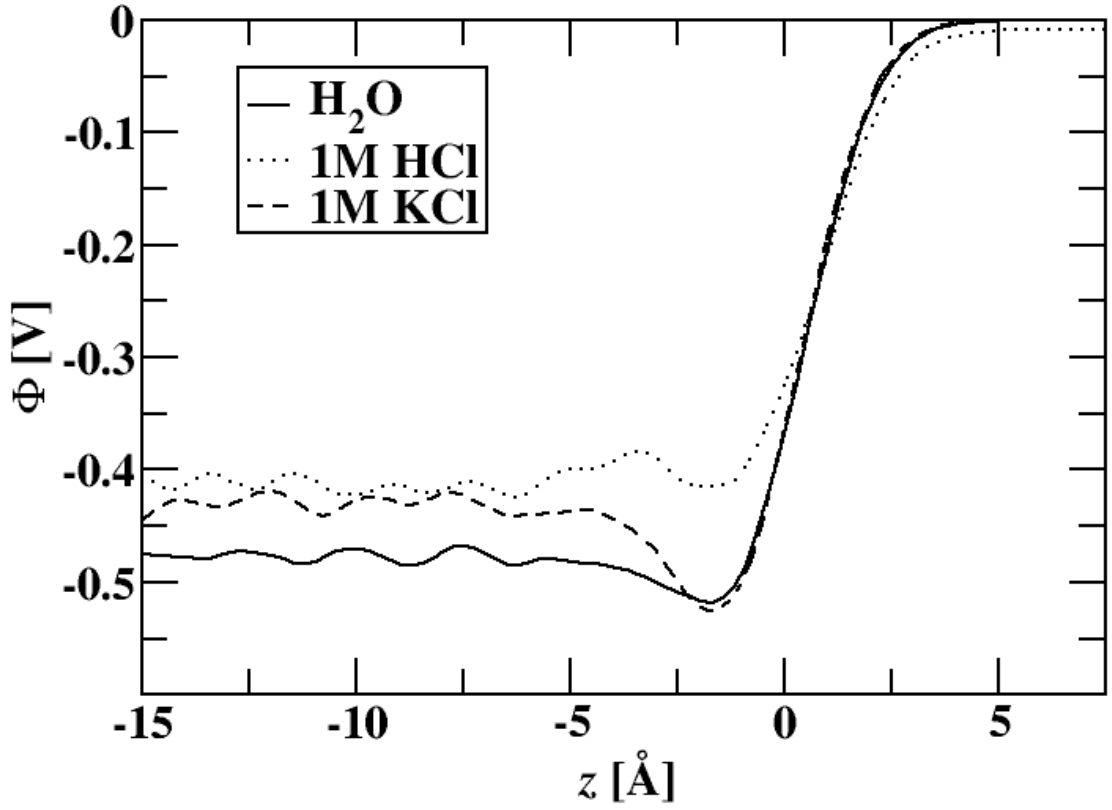

FIG. 8.

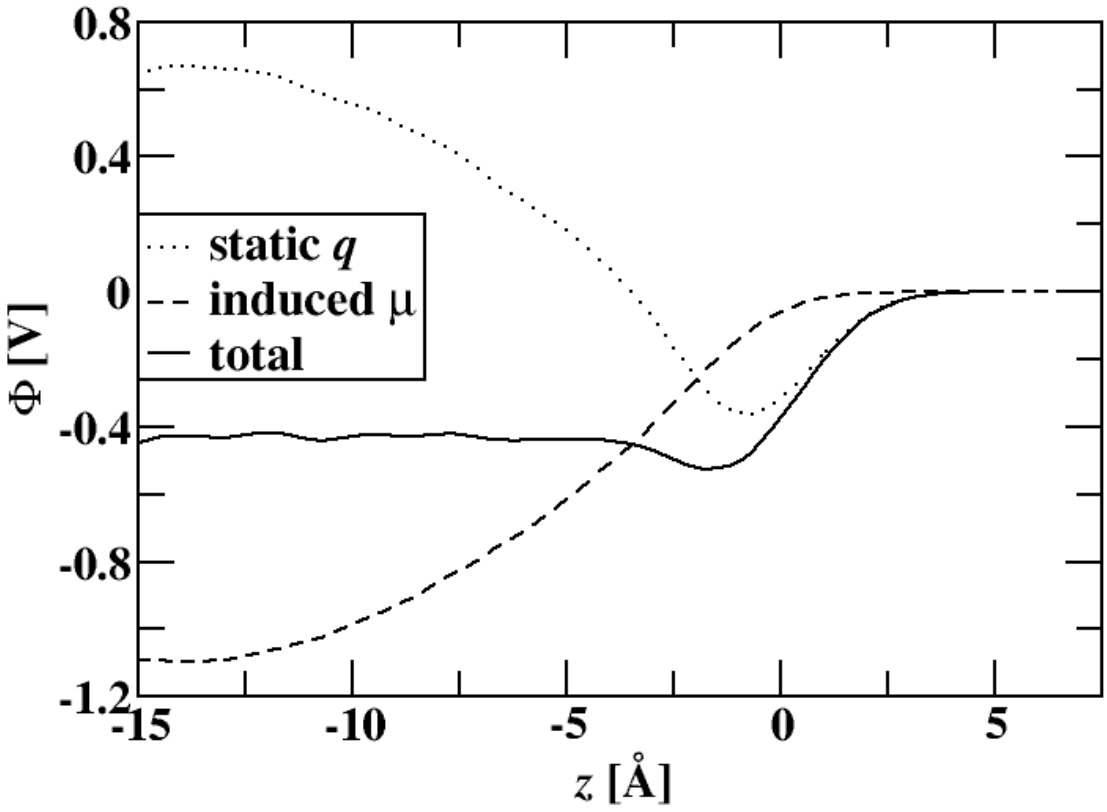

FIG. 9.

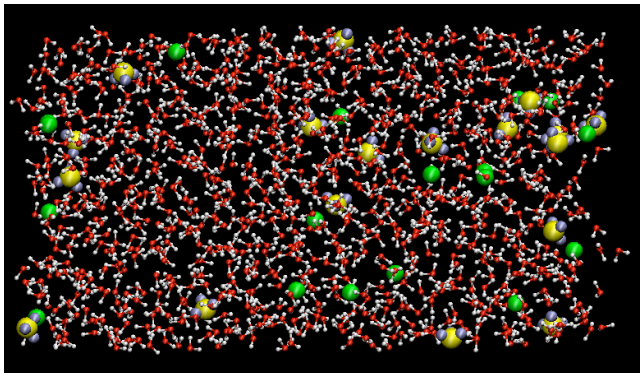

a) 1M HCl

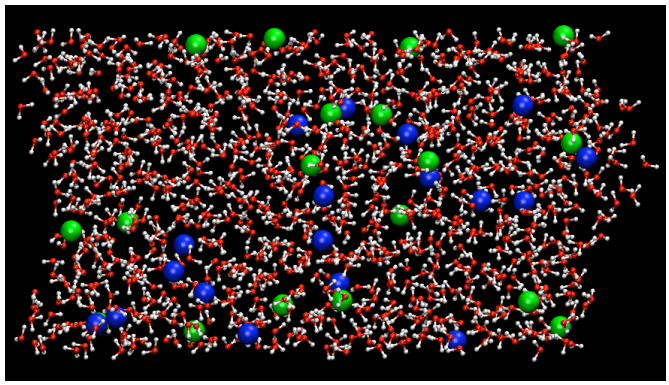

b) 1M KCl

FIG. 10.

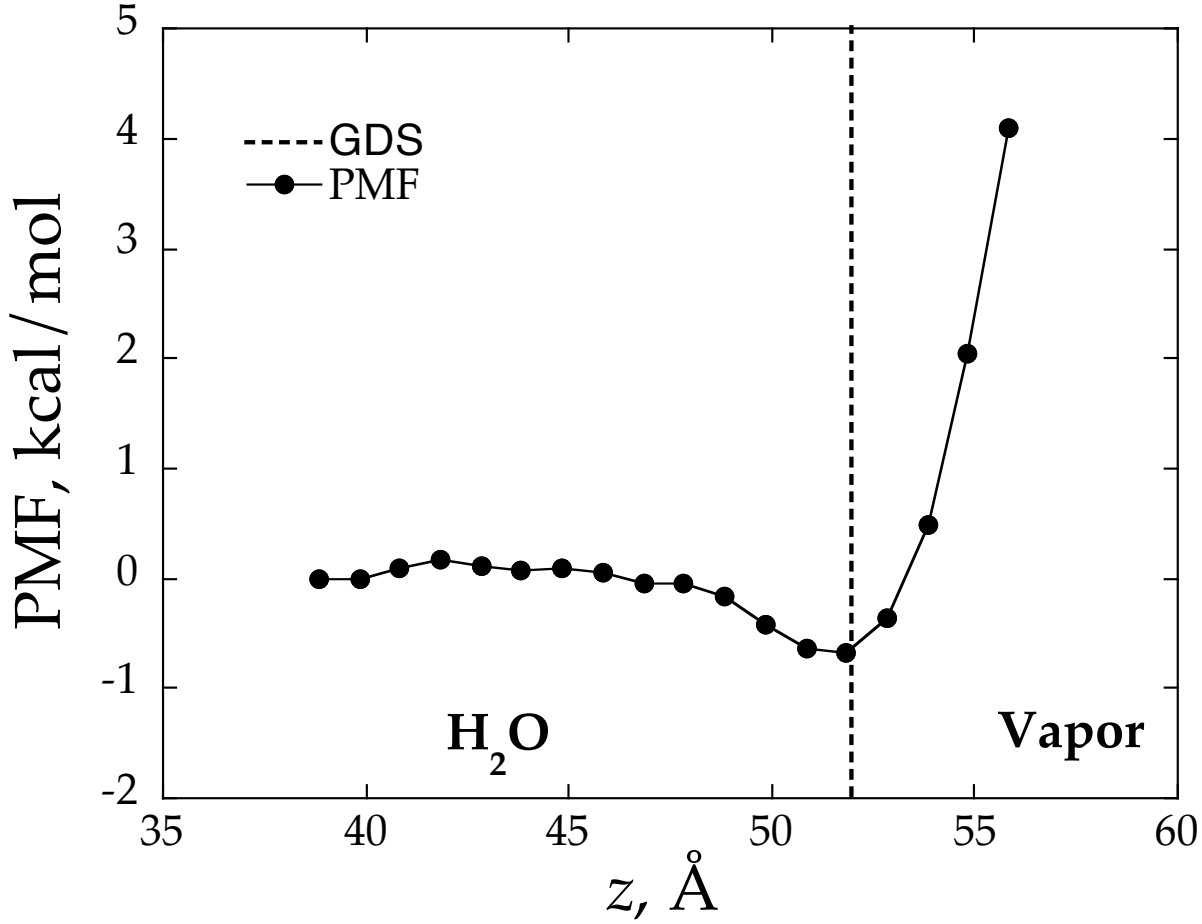

FIG. 11.

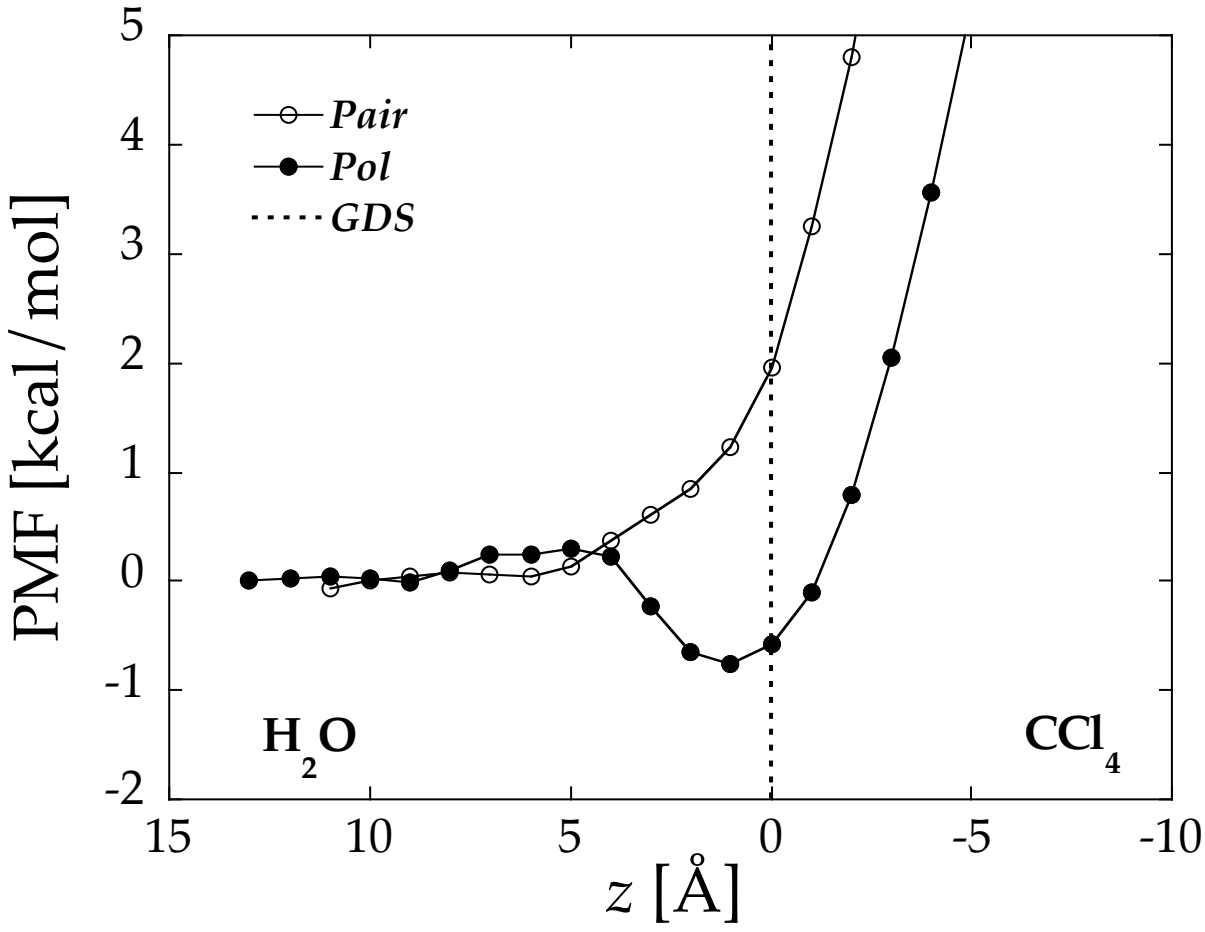

Tables

Table 1. Interfacial Widths (δ) and Total Dipole Moments in the Water Bulk and at the GDS for Various Water Molecules.

	BLYP	D-C	TIP4P	SPC-FW	TIP4P-POL2[a]	TIP4P-FQ[a]
δ (Å)	0.78	1.45	1.56	1.45	1.782	1.575
ρ_l (g/cm^3)	0.857	0.98	0.98	1.00	0.995	1.007
$\langle \mu_{\mathrm{Bulk}}(\mathrm{D}) \rangle$	3.02	2.74	2.18	2.39	2.48	2.64
$\langle \mu_{\mathrm{GDS}}(\mathrm{D}) \rangle$	2.6	2.53	2.18	2.39	2.38	2.41

[a] Results taken from ref. 15.

Table 2. Hydrogen Bond Populations for the Water Bulk and Interface for Models Tested.

BLYP[a] TIP4P D-C	0D		1D		2D	
	Bulk	Interface	Bulk	Interface	Bulk	Interface
0A	0.8	3.5	2.9	8.3	2.1	2.3
	1.1	2.6	5.5	9.3	3.4	3.3
	0.8	3.4	3.6	7.6	2.4	2.4
1A	3.5	8.4	19.3	34.2	19.8	14.8
	3.7	6.4	21.1	27.6	17	14.2
	2.8	6.1	17.7	26.0	17.5	14.8
2A	2.2	2.2	18.3	13.8	30.8	12.5
	3.2	3.4	21.3	18.4	22.0	14.0
	2.4	2.6	20.7	17.9	30.0	18.2

[a] Results taken from ref. 15.

Table 3. Average Oxygen-Oxygen Distance in the Water Bulk and Between the GDS and 2δ from the GDS.[a]

Model	$\langle r_{OO} \rangle_{bulk}$	$\langle r_{OO} \rangle_{interface}$
BLYP	2.93 Å	2.96 Å
TIP4P	2.930 Å	2.922 Å
D-C	2.900 Å	2.909 Å
SPC-FW	2.866 Å	2.863 Å
TIP4P-POL2[b]	2.96 Å	2.93 Å
TIP4P-FQ[b]	2.99 Å	2.98 Å

[a] Uncertainties are smaller than the last digit reported.

[b] Taken from ref. 15.

References

(1) Jungwirth, P.; Tobias, D. J. *Chem. Rev.* **2006**, *106*, 1259-1281.

(2) Chang, T. M.; Dang, L. X. *Chem. Rev.* **2006**, *106*, 1305-1322.

(3) Rivera, J. L.; Starr, F. W.; Paricaud, P.; Cummings, P. T. *J. Chem. Phys.* **2006**, *125*.

(4) Motakabbir, K. A.; Berkowitz, M. L. *Chem. Phys. Lett.* **1991**, *176*, 61-66.

(5) Saturo, I.; Izvekov, S.; Voth, G. A. *J. Chem. Phys.* **2007**, *126*, 124505(1-13).

(6) Wilson, K. R.; Rude, B. S.; Catalano, T.; Schaller, R. D.; Tobin, J. G.; Co, D. T.; Saykally, R. J. *J. Phys. Chem. B* **2001**, *105*, 3346-3349.

(7) Wilson, K. R.; Schaller, R. D.; Co, D. T.; Saykally, R. J.; Rude, B. S.; Catalano, T.; Bozek, J. D. *J. Chem. Phys.* **2002**, *117*, 7738-7744.

(8) Richmond, G. L. *Chem. Rev.* **2002**, *102*, 2693-2724.

(9) Gopalakrishnan, S.; Liu, D. F.; Allen, H. C.; Kuo, M.; Shultz, M. J. *Chem. Rev.* **2006**, *106*, 1155-1175.

(10) Du, Q.; Superfine, R.; Freysz, E.; Shen, Y. R. *Phys. Rev. Lett.* **1993**, *70*, 2313-2316.

(11) Shultz, M. J.; Baldelli, S.; Schnitzer, C.; Simonelli, D. *J. Phys. Chem. B* **2002**, *106*, 5313-5324.

(12) Kemnitz, K.; Bhattacharyya, K.; Hicks, J. M.; Pinto, G. R.; Eisenthal, K. B.; Heinz, T. F. *Chem. Phys. Lett.* **1986**, *131*, 285-290.

(13) Ghosal, S.; Hemminger, J. C.; Bluhm, H.; Mun, B. S.; Hebenstreit, E. L. D.; Ketteler, G.; Ogletree, D. F.; Requejo, F. G.; Salmeron, M. *Science* **2005**, *307*, 563-566.

(14) Raymond, E. A.; Richmond, G. L. *J. Phys. Chem. B* **2004**, *108*, 5051-5059.

(15) Kuo, I. F. W.; Mundy, C. J.; Eggimann, B. L.; McGrath, M. J.; Siepmann, J. I.; Chen, B.; Vieceli, J.; Tobias, D. J. *J. Phys. Chem. B* **2006**, *110*, 3738-3746.

(16) Kuo, I. F. W.; Mundy, C. J. *Science* **2004**, *303*, 658-660.

(17) Rick, S. W.; Stuart, S. J.; Berne, B. J. *J. Chem. Phys.* **1994**, *101*, 6141-6156.

(18) Randles, J. E. B. *Phys. Chem. Liq.* **1977**, *7*, 107-179.

(19) Dang, L. X.; Chang, T. M. *J. Phys. Chem. B* **2002**, *106*, 235-238.

(20) Wilson, M. A.; Pohorille, A.; Pratt, L. R. *J. Chem. Phys.* **1988**, *88*, 3281-3285.

(21) Wick, C. D.; Dang, L. X. *J. Phys. Chem. B* **2006**, *110*, 6824-6831.

(22) Chang, T. M.; Dang, L. X. *J. Chem. Phys.* **1996**, *104*, 6772-6783.

(23) Jorgensen, W. L.; Chandrasekhar, J.; Madura, J. D.; Impey, R. W.; Klein, M. L. *J. Chem. Phys.* **1983**, *79*, 926-935.

(24) Dang, L. X.; Chang, T. M. *J. Chem. Phys.* **1997**, *106*, 8149-8159.

(25) Wu, Y. J.; Tepper, H. L.; Voth, G. A. *J. Chem. Phys.* **2006**, *124*.

(26) Essmann, U.; Perera, L.; Berkowitz, M. L.; Darden, T.; Lee, H.; Pedersen, L. G. *J. Chem. Phys.* **1995**, *103*, 8577-8593.

(27) Tuckerman, M.; Berne, B. J.; Martyna, G. J. *J. Chem. Phys.* **1992**, *97*, 1990-2001.

(28) Berendsen, H. J. C.; Postma, J. P. M.; Vangunsteren, W. F.; Dinola, A.; Haak, J. R. *J. Chem. Phys.* **1984**, *81*, 3684-3690.

(29) Ryckaert, J. P.; Ciccotti, G.; Berendsen, H. J. C. *Journal Of Computational Physics* **1977**, *23*, 327-341.

(30) Martyna, G. J.; Klein, M. L.; Tuckerman, M. *J. Chem. Phys.* **1992**, *97*, 2635-2643.

(31) Mundy, C. J.; Kuo, I. F. W. *Chem. Rev.* **2006**, *106*, 1282-1304.

(32) Becke, A. D. *Physical Review A* **1988**, *38*, 3098-3100.

(33) Lee, C. T.; Yang, W. T.; Parr, R. G. *Physical Review B* **1988**, *37*, 785-789.

(34) Chen, B.; Xing, J. H.; Siepmann, J. I. *J. Phys. Chem. B* **2000**, *104*, 2391-2401.

(35) Lee, H. S.; Tuckerman, M. E. *J. Chem. Phys.* **2006**, *125*.

(36) Todorova, T.; Seitsonen, A. P.; Hutter, J.; Kuo, I. F. W.; Mundy, C. J. *J. Phys. Chem. B* **2006**, *110*, 3685-3691.

(37) Grossman, J. C.; Schwegler, E.; Draeger, E. W.; Gygi, F.; Galli, G. *J. Chem. Phys.* **2004**, *120*, 300-311.

(38) VandeVondele, J.; Mohamed, F.; Krack, M.; Hutter, J.; Sprik, M.; Parrinello, M. *J. Chem. Phys.* **2005**, *122*.

(39) Kuo, I. F. W.; Mundy, C. J.; McGrath, M. J.; Siepmann, J. I.; VandeVondele, J.; Sprik, M.; Hutter, J.; Chen, B.; Klein, M. L.; Mohamed, F.; Krack, M.; Parrinello, M. *J. Phys. Chem. B* **2004**, *108*, 12990-12998.

(40) McGrath, M. J.; Siepmann, J. I.; Kuo, I. F. W.; Mundy, C. J. *Mol. Phys.* **2006**, *104*, 3619-3626.

(41) McGrath, M. J.; Siepmann, J. I.; Kuo, I. F. W.; Mundy, C. J.; VandeVondele, J.; Hutter, J.; Mohamed, F.; Krack, M. *J. Phys. Chem. A* **2006**, *110*, 640-646.

(42) McGrath, M. J.; Siepmann, J. I.; Kuo, I. F. W.; Mundy, C. J.; VandeVondele, J.; Hutter, J.; Mohamed, F.; Krack, M. *Chemphyschem* **2005**, *6*, 1894-1901.

(43) McGrath, M. J.; Siepmann, J. I.; Kuo, I. F. W.; Mundy, C. J.; VandeVondele, J.; Sprik, M.; Hutter, E.; Mohamed, F.; Krack, M.; Parrinello, M. *Comput. Phys. Commun.* **2005**, *169*, 289-294.

(44) Badyal, Y. S.; Saboungi, M. L.; Price, D. L.; Shastri, S. D.; Haeffner, D. R.; Soper, A. K. *J. Chem. Phys.* **2000**, *112*, 9206-9208.

(45) Sokhan, V. P.; Tildesley, D. J. *Mol. Phys.* **1997**, *92*, 625-640.

(46) Paluch, M. *Adv. Colloid Interface Sci.* **2000**, *84*, 27-45.

(47) Jeon, J.; Lefohn, A. E.; Voth, G. A. *J. Chem. Phys.* **2003**, *118*, 7504-7518.

(48) Stern, H. A.; Rittner, F.; Berne, B. J.; Friesner, R. A. *J. Chem. Phys.* **2001**, *115*, 2237-2251.

(49) Wick, C. D.; Dang, L. X.; Jungwirth, P. *J. Chem. Phys.* **2006**, *125*.

(50) Dang, L. X. *J. Chem. Phys.* **2003**, *119*, 6351-6353.

(51) Dang, L. X. *J. Phys. Chem. B* **2002**, *106*, 10388-10394.

(52) Petersen, M. K.; Iyengar, S. S.; Day, T. J. F.; Voth, G. A. *J. Phys. Chem. B* **2004**, *108*, 14804-14806.

(53) Petersen, P. B.; Saykally, R. J. *J. Phys. Chem. B* **2005**, *109*, 7976-7980.

(54) Wick, C. D.; Dang, L. X. *J. Chem. Phys.* **2007**, *126*, 134702 (1-4).

(55) Duffy, E. M.; Severance, D. L.; Jorgensen, W. L. *J. Am. Chem. Soc.* **1992**, *114*, 7535-7542.